

# Neoclassical Resistivity Revisited

T. N. Todd<sup>1</sup>, M. C. R. Andrade<sup>2</sup>, G. O. Ludwig and J. G. Ferreira

Instituto Nacional de Pesquisas Espaciais (INPE/MCT)  
P.O.Box 515, 12245-970, São José dos Campos-SP, Brazil

<sup>1</sup>UKAEA Dounreay, Caithness, KW14 7TZ, Scotland

**Abstract:** The inclusion of the trapped particle fraction in the expression for the conductivity of the plasma near the minor axis of a tokamak (where the inverse aspect ratio  $\epsilon$  tends to 0) is usually shown to result in a cusp in central current density, representing an unphysical “catastrophe”. Here we revisit the drift kinetics of the electron distribution function, including a usually neglected term accounting for the finite toroidal electric field, which accelerates the parallel component of the electron velocity. This term competes with the usual collisionality term in detrapping a substantial fraction of the electrons at finite  $\epsilon$  and in the limit of vanishing  $\epsilon$ , the whole population. We develop an analysis of the electric field detrapping effect and its convolution with the collisionality term, leading to an illustration of the modified profile of the current density in the region near the minor axis of a typical tokamak

*PAC Nos 52.55.Fa, 52.20 Dq, 52.25Fi*

---

<sup>1</sup> e-mail: tom.todd@ukaea.org.uk

<sup>2</sup> e-mail: mcr@plasma.inpe.br

## 1. Introduction

This paper develops a comprehensive expression for the neoclassical current density in toroidal devices of tokamak ordering, accounting for the acceleration effect of the toroidal electric field in reducing the pitch angle of trapped electrons such that they become untrapped; the effect of launch-point averaging in reducing the trapped particle fraction on a given flux surface, and the increase in bounce period brought about by the combination of the toroidal electric field and the non-linearity of large-excursion banana orbits. The initial sections outline the electric field effect in terms of single particle analysis and the subsequent sections develop this further to account for a Maxwellian distribution of particle velocity, launch point averaging of the trapped particle fraction, variation of the bounce period with the poloidal excursion of the banana orbits, and finally the convolution with collisionality.

It is shown that including the collisionality or the toroidal electric field alone removes the “catastrophe” of infinite current density gradient otherwise theoretically predicted at the magnetic axis of the tokamak according to the usual neoclassical theory [1-2]. With both terms active, the effect on the current density profile, especially the central and peripheral regions, is quite significant given parameters typical of many present-day experiments.

The implications for experimental interpretations concerning such neoclassical effects as bootstrap current [3], neoclassical tearing modes [4], current drive and so on are also potentially of significance but are not elaborated here. Also finite trapped particle fraction on the magnetic axis resulting from orbit effects like kidney-bean (aka potato) orbits [5-6] is not included in this work. This paper addresses the role of the driven electric field in detrapping particles that would in conventional neoclassical theory exhibit a trapped particle fraction,  $f_t$ , falling to zero at the magnetic axis as  $f_t \approx \sqrt{\epsilon}$ . It should be also underlined that the topology of orbits for highly energetic ions with large excursions over the plasma cross section is not considered here. Our trapped region is thus symmetric in the  $v_{//} - v_{\perp}$  space, different from ref.[7], and modified due to the presence of the driven electric field.

The structure of the paper is as follows:

1. Introduction
2. Mono-energetic particles launched at the outer midplane
3. Integration over velocity distribution
4. Launch point averaging of trapped particle fraction
5. Current density profiles
6. Collisionality effects
7. Conclusions
8. References
9. Appendices

## 2. Mono-energetic particles launched at the outer midplane

For a circular plasma in the large aspect ratio approach, the combination of the magnetic mirror force and the parallel electric field, approximately given by the toroidal component  $E_\phi$ , results in a potential energy curve resembling a tilted sine wave, as developed in Appendix 1. This yields an expression for the total potential energy versus the coordinate  $\phi/q$ , or equivalently the poloidal angle  $\theta$ , as follows:

$$\delta E_{//}(\phi) = \frac{E_\perp}{A} \left[ 1 - \cos\left(\frac{\phi}{q}\right) \right] - qeE_\phi R_0 \frac{\phi}{q}, \quad (1)$$

described in a toroidal coordinate system  $(r, \theta, \phi)$  where  $r$  represents the radial coordinate on the poloidal plane,  $\theta$  is the poloidal angle representing the excursion of a field line around the minor circumference, and  $\phi$  is the toroidal angle representing excursions around the symmetry axis. This expression contains an approximation in the first term, as explained in Appendix 1. In Eq.(1),  $A$  is the local aspect ratio ( $A = R_0/r$ ),  $R_0$  is the tokamak geometric radius,  $e$  is the electronic charge and  $q$  the safety factor. The potential energy described in Eq.(1) is plotted in figure 1 for a range of normalised electric fields  $x$  given by  $x = \{0, 0.2, 0.5, 0.6, 0.724611, 0.8, 0.9, 1\}$ , with  $x$  being defined as  $x = qeE_\phi R_0 / (\epsilon E_\perp)$ .  $\epsilon$  is the local inverse aspect ratio;  $\epsilon = A^{-1}$ .

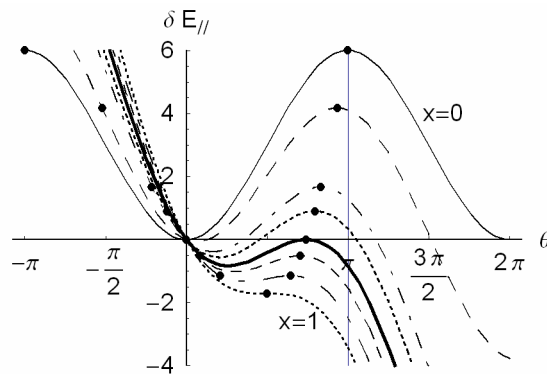


Figure 1: Potential Energy Curve for different normalised electric field values "x". The thicker trace corresponds to the critical value  $x_c=0.7246$  for  $\theta=0$ .

If  $x = 1$ , the potential energy has a point of inflexion at  $\theta = \pi/2$ , that is the electrostatic and magnetic forces balance each-other. Accordingly for finite values of  $x$  below unity there arises a critical initial parallel energy in order that a particle launched from  $\theta = 0$  can overcome the potential barrier (ie. to become untrapped):

$$E_{//c} = E_{\perp} \varepsilon \left[ 1 + \sqrt{1 - x^2} - x (\pi - \arcsin(x)) \right] . \quad (2)$$

The region of trapping we are interested in lies within the poloidal range  $-\pi < \theta < \pi$ . Dots above  $\pi/2$  in figure 1, represent the peak energy for different electric field values (or  $x$  values). Dots below  $\pi/2$  represent the equivalent upstream point.

The critical toroidal electric field for particles launched from the outboard midplane ( $\theta = 0$ ) with no parallel velocity is given by solving the expression for  $E_{//c} = 0$ , with the result:

$$E_{\phi} \geq 0.7246 \varepsilon E_{\perp} / (eqR_0) . \quad (3.a)$$

The thicker trace, in figure 1, corresponds to this critical normalised electric field  $x_c = 0.7246$ .

In the same way, for a given electric field, there will also be a critical perpendicular energy below which no particles launched at the outboard midplane with any  $E_{//}$  are trapped. This critical perpendicular energy is defined by:

$$E_{\perp c} \leq E_{\phi} e q R_0 / (0.7246 \varepsilon) \quad (3.b)$$

The expression for  $E_{//c}$ , given in (2), can be approximated without significant loss of accuracy by:

$$E_{//c} = 2E_{\perp} \varepsilon (1 - x/0.725) \quad (4)$$

Noting that  $x = qeE_{\phi}R_0 / (\varepsilon E_{\perp}) \approx 0.725$  corresponds, in the case  $\theta = 0$ , to the critical value of  $E_{\perp}$  ( $E_{\perp c}$  being constant for each flux surface), Eq.(4) can be rewritten as:

$$E_{//c} / E_{\perp} = 2\varepsilon (1 - E_{\perp c} / E_{\perp}) \quad (5)$$

This expression will be used in the next section in the integration of the velocity distribution function over the velocity space in order to estimate the trapped particle fraction for particles launched at the outer midplane under the action of the driven electric field.

### 3. Integration over velocity distribution

The part of the velocity distribution representing particles with perpendicular velocities below the critical perpendicular energy contributes nothing to the trapped particle

fraction. This critical  $E_{\perp}$  (ie.  $E_{\perp c}$ ) corresponds to a critical  $v_{\perp}$ , here termed  $v_{\perp c}$ . This is shown diagrammatically in figure 2 for a representative series of values of  $v_{\perp c}$ .

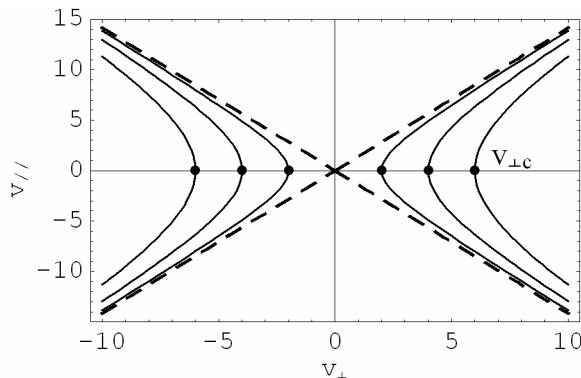


Figure 2: Trapped particle boundaries in velocity space for various values of the normalised electric field  $x$ . The dots indicate the chosen values of  $v_{\perp c}$ , and the dashed lines represent the boundary when  $E_{\phi}=0$ .

The ratio  $v_{||}/v$  represents, for high perpendicular velocities, the trapped particle fraction, and corresponds to the sine of the asymptotic complementary pitch angle (ie. the angle formed by a dashed line and the horizontal axis in figure 2). This ratio is conventionally accepted as given by  $f_t(r) = \sqrt{2\varepsilon(r)/(1+\varepsilon(r))}$  [8], and may be obtained by integrating a Maxwellian over the trapped boundary delimited by the dashed lines in velocity space in figure 2. Furthermore, this result represents the trapped particle fraction for launch points at the outer midplane, which is the assumption in the calculations described in the present section. The effect of different launch points on the resulting  $f_t(r)$  will be considered in section 4.

In the presence of the electric field, the trapped boundary is modified into the regions defined by the full lines in figure 2, which have a lower limit in  $v_{\perp}$  corresponding to the critical value  $v_{\perp c}$ . The total trapped particle fraction on a flux surface is then obtained by integrating the velocity distribution, still considered as a Maxwellian, over this new boundary. This integration is shown in full in Appendix 2, resulting in the following expression for the trapped particle fraction:

$$f_t(r) = \exp(-v(r)^2) \sqrt{\frac{2\varepsilon(r)}{1+2\varepsilon(r)}} \quad , \quad (6)$$

where  $v(r) = \sqrt{E_{\perp c}(r)/T_e(r)}$ , in the exponential factor, introduces the modification due to the electric field.  $T_e(r)$  represents the electron temperature profile. Note that when the electric field  $E_{\phi} = 0$ , then  $E_{\perp c} = 0$  and  $v(r) = 0$ . In this case, the trapped particle fraction reduces to

the large aspect ratio expression in the absence of the electric field,  $f_t(r) = \sqrt{2\varepsilon(r)/(1+2\varepsilon(r))}$ , which is slightly different from the usual expression mentioned above,  $\sqrt{2\varepsilon(r)/(1+\varepsilon(r))}$ . This is due to the fact that in this paper an approximation for the parallel potential energy has been adopted.

In order to make the estimate of the trapped particle fraction profile consistent with a determined current density and for given electron temperature profiles, an iterative process for the current density  $j(r)$  is developed as described below.

Initially, a first guess for  $j(r)$  is considered and the central current density  $j_0$  is chosen in order to support a particular value for  $q_0$ , say  $q_0=1.0$ . This then sets the value of  $E_\phi$  for a calculation of  $j(r)$ , allowing an intuitively interpretable superposition of current density profiles with the same central current density, for various values of control parameters such as  $T_{e0}$ . (Of course, since central current density is thus kept constant while the current profile shape varies, the total plasma current and the profile of safety factor  $q$  are in general not constant). Thus (ignoring Shafranov shift, diamagnetism and paramagnetism, skin effect and tearing modes lowering the central electric field compared to the surface value),

$$j_0 = (2/\mu_0) B_\phi / (q_0 R_0) \quad , \quad (7)$$

leading to a toroidal electric field given by:

$$E_\phi = \frac{j_0}{\sigma_{\text{Spitzer}}(0)} \quad . \quad (8)$$

In Eq. (7),  $B_\phi$  represents the toroidal magnetic field and the Spitzer conductivity  $\sigma_{\text{Spitzer}}$ , in (8), is described as:

$$\sigma_{\text{Spitzer}}(r) = \frac{3(2\pi)^{3/2} \varepsilon_0^2 T_e(r)^{3/2}}{\sqrt{m_e} e \ln \Lambda} \Lambda_E(Z_{\text{eff}}), \quad (9)$$

where  $m_e$  and  $e$  are respectively the electron mass and charge, and  $\Lambda_E(Z_{\text{eff}})$  represents the correction to account for impurities in the plasma given by [9]:

$$\Lambda_E(Z_{\text{eff}}) = \frac{3.40}{Z_{\text{eff}}} \left( \frac{1.13 + Z_{\text{eff}}}{2.67 + Z_{\text{eff}}} \right) \quad . \quad (10)$$

The electron temperature profile adopted here was taken to be of the form:

$$T_e(r) = (T_{e0} - T_{\text{edge}}) \left[ 1 - \left( \frac{r}{a} \right)^2 \right]^{\alpha_T} + T_{\text{edge}} \quad . \quad (11)$$

The neoclassical current density, when the plasma collisionality is not taken into account, is approximately given by:

$$j(r) = \sigma_{\text{Spitzer}}(r) (1 - f_t(r)) E_\phi \quad . \quad (12)$$

The trapped particle fraction is then calculated through Eq.(6) where  $E_{\perp c}$  is obtained from (3.b) replacing the inequality by the equal sign. In this equation we have also dropped the electronic charge in order to obtain the perpendicular critical energy in eV. Note that the critical  $x$  value for  $\theta = 0$  is  $x_c = 0.7246$ . In each case there is only  $q(r)$  which has to be determined. The safety factor profile that enters the equation for  $E_{\perp c}$  is estimated using the following expression:

$$q(r) = \varepsilon^2 R_0 B_\phi / \left( \mu_0 \int_0^r r' j(r') dr' \right) \quad (13)$$

with  $j(r)$  being given in the first iteration by our first guess introduced in the process.

At this point, having defined all the necessary parameters, the new current density profile can thus be obtained from (12). This new current density is reintroduced in the iterative process and all the calculations described above are repeated until  $j(r)$  converges within a given tolerance. The central current density  $j_0$  and the toroidal electric field  $E_\phi$  are kept constant for all iterations.

Figure 3 shows resulting profiles of trapped particle fraction for different central electron temperatures as listed in table 1. The respective toroidal electric fields in each of these cases are also listed in the same table. The other fixed parameters used in the calculation are listed in table 2.

$T_{e0}$ (eV)	50	80	200	2000
$E_\phi$ (V/m)	7.1	3.5	0.89	0.03

Table 1: Central electron temperatures and electric fields obtained for trapped particle calculation in figure 3.

$T_{\text{edge}}$	$\alpha_T$	$Z_{\text{eff}}$	$B_\phi$	$q_0$	$R_0$	$R_0/a$
$1.0 \times 10^{-3} T_{e0}$	2	1	1 T	1	0.56 m	3.5

Table 2: Set of parameters used for trapped particle and current density profile calculations.

It can be observed in figure 3 that for  $T_{e0} = 50$  eV there is essentially a simple Spitzer behaviour, (ie. almost no trapping), due to the very effective action of the electric field in low temperature plasmas. In the other cases shown in the figure, although particles are trapped in a significant ratio, the electric field continues to play a significant role in detrapping them. This detrapping effect takes place over the whole plasma cross section becoming more

evident, in the case of high temperature plasmas, in the plasma edge, where the temperature is lower. In the plasma centre, as the temperature increases, the detrapping of particles occurs closer and closer to the magnetic axis and it is hardly observed when  $T_{e0} = 2$  keV. However, it is always sufficient, even in high temperature plasmas, to eliminate the singular behaviour in this region, otherwise present when there is no electric field. The crosses in the plot represent the trapped particle fraction for  $E_\phi = 0$  and circular plasmas, given by  $f_t(r) = \sqrt{2\varepsilon(r)/(1+2\varepsilon(r))}$ . Note that for  $T_{e0} = 2$  keV,  $f_t$  is nearly coincident with this result but the electric field is still acting. Its effect is better observed, in this case, in the plasma edge.

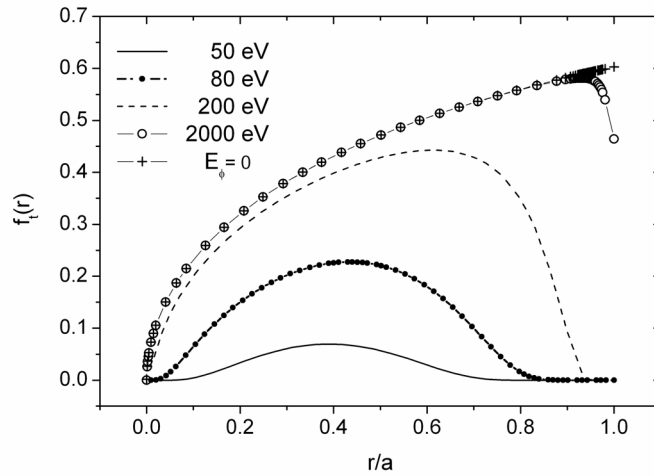


Figure.3: Trapped particle fraction for various central electron temperatures under the effect of the toroidal electric field, and in the case when there is no electric field (crosses). In this figure only outboard midplane launch points are considered.

#### 4. Launch Point Averaging of Trapped Particle Fraction

In this section the theory is developed to account for the different launch points of the particles around the poloidal circumference, still assuming a Maxwellian distribution at each launch point.

Any charged particle born at a point can only be co-passing, counter-passing or trapped, and in the absence of an electric field will map out the whole orbit associated with whichever of these (nested) classes it represents, wherever it started from.

In the situation of interest here, the co-passing particles are continuously accelerated by the toroidal electric field and hence develop increasingly inwardly displaced drift orbit surfaces. Those born as counter-passing are decelerated by the electric field until they reflect off one of the peaks of the potential energy curve. They will not become trapped unless they lose parallel energy by some other mechanism (not considered here) within the potential energy well where they were reflected, and hence they just become part of the continuously

accelerating co-passing class. While decelerating, these counter-passing particles progressively lose their characteristic outward drift orbit displacement, of course. This leaves the ones born as trapped particles, necessarily with turning points between the poloidal angle of formation (equivalently the major radius of formation) and the downstream point of highest potential energy (which is a function of their  $E_{\perp}$ ). Neglecting collisions and other energy loss or gain processes, these will stay trapped but they will suffer net  $\nabla B$  drift towards the midplane, owing to the lack of up-down symmetry in the banana orbits.

The first thing to note in developing the calculation of trapped particle fraction is that, as noted in figure 1, the minimum of the potential energy function is not at the outboard midplane but is shifted “downstream” by the toroidal electric field (oppositely for the ions and electrons, of course). Appendix 3 covers the details, beginning with the derivation of the critical parallel energy for detrapping as a function of the poloidal angle of the launch point  $\theta$ :

$$E_{//c}(\theta) = E_{\perp} \varepsilon \left( 1 + \sqrt{1 - x^2} - x (\pi - \arcsin(x)) - 1 + \cos(\theta) + x\theta \right). \quad (14)$$

This expression already includes the corrections to the potential energy curve for the shift of the potential energy minimum due to the electric field.

Equation (14) can be approximated, as developed in details in Appendix 3, by the following expression:

$$E_{//c}(\theta) = E_{\perp} \varepsilon (1 + \cos \theta) \left[ 1 - \frac{x}{x_c(\theta)} \right], \quad (15)$$

allowing an analytical form for the trapped particle fraction related to a given launch point, similar to the derivation used in the case  $\theta = 0$ :

$$f_t(r, \theta) = \exp(-v(r, \theta)^2) \sqrt{\frac{\varepsilon(r) (1 + \cos \theta)}{1 + \varepsilon(r) (1 + \cos \theta)}}, \quad (16)$$

with  $v(r, \theta) = \sqrt{E_{\perp c}(r, \theta)/T_e(r)} = v_{\perp c}(r, \theta)/v_{th}(r)$ , and  $v_{th}(r)$  representing the thermal velocity. The value of  $x_c(\theta)$ , used in the calculation of  $v_{\perp c}(r, \theta)$ , is obtained by solving numerically Eq.(14) when  $E_{//c}(\theta) = 0$ .

This and the exact calculation, here denominated “complete”, obtained numerically when the potential energy curve is given by the full form described by Eq.(14), are then integrated over the poloidal circumference to produce the full average trapped particle fraction, generating graphical results such as those of figures 4 and 5. These figures show, respectively, the variation of the trapped particle fraction with the inverse aspect ratio plotted in both linear and logarithmic scales. The plots show also the comparison of  $f_t$  obtained from

both methods (complete and approximated) for fixed values of  $h$ , which is a form for the normalised electric field described by  $h(r) = q(r) V_{loop} / (2\pi T_e(r))$ . The normalisation here refers to the electron temperature profile while the variable  $x$  refers to the electric field normalised to the perpendicular energy. The parameter “ $h$ ” is considered to vary from  $1 \times 10^{-6}$  to 1, covering the full range of parameters for large aspect ratio machines (see details for the definition of this parameter in Appendix 3).

We can observe from these figures that  $f_t$  does not present the usual singular behaviour as  $\epsilon \rightarrow 0$ , and that the role of the electric field in detrapping particles is actually more effective when the temperature is lower or, of course, when the electric field is higher (or in other words, when  $h$  increases). When  $h$  is low, the trapped particle profile approaches the usual well known behaviour as shown in figure 4(a).

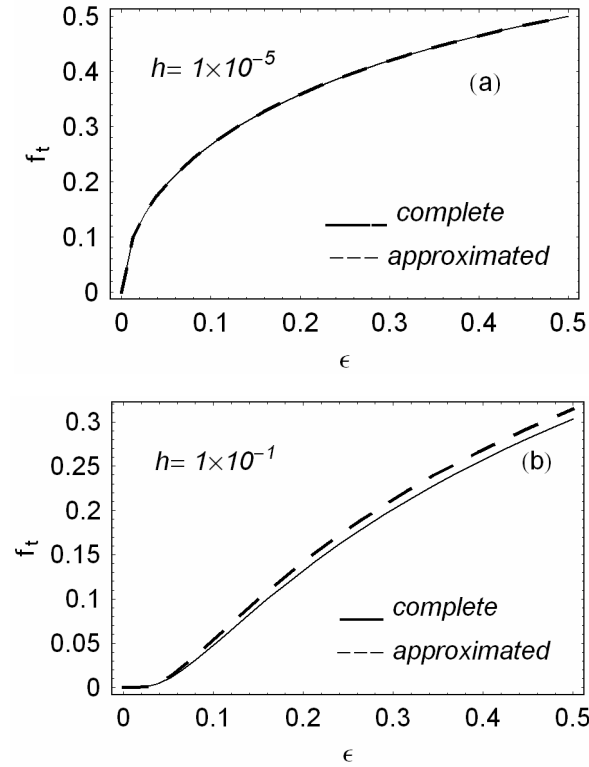


Figure 4: Variation of  $f_t$  with inverse aspect ratio in linear scale and fixed values of “ $h$ ”. The plot compares  $f_t$  when the complete or approximated forms for  $E_{//c}$  are used in the calculation.

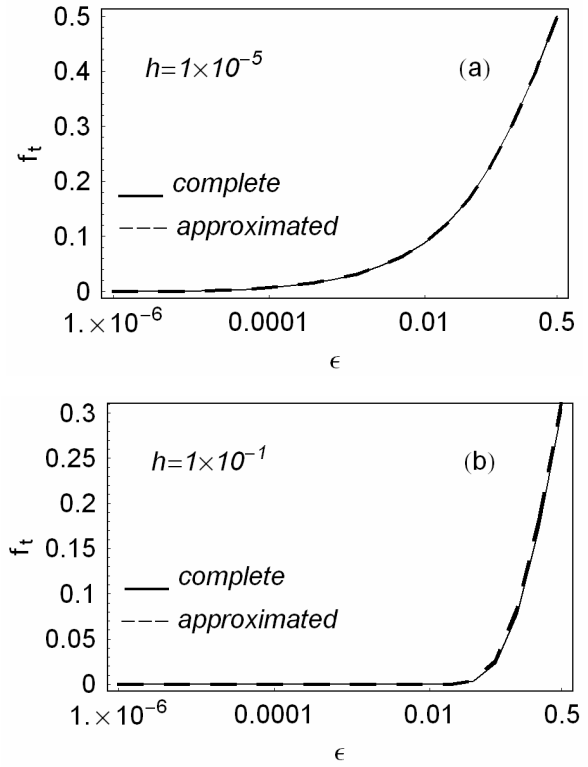


Figure 5: Variation of  $f_t$  with inverse aspect ratio in logarithmic scale and fixed values of “ $h$ ”. The plot compares  $f_t$  when the complete or approximated forms for  $E_{//c}$  are used in the calculation.

Figure 6 shows the trapped particle fraction obtained again from both methods, but now plotted against “ $h$ ” and for fixed inverse aspect ratios such as  $\epsilon = 0.01$  and  $\epsilon = 0.1$ . These figures reinforce the fact that as the ratio of the electric field to the electron temperature increases, the detrapping of particles is more effective.

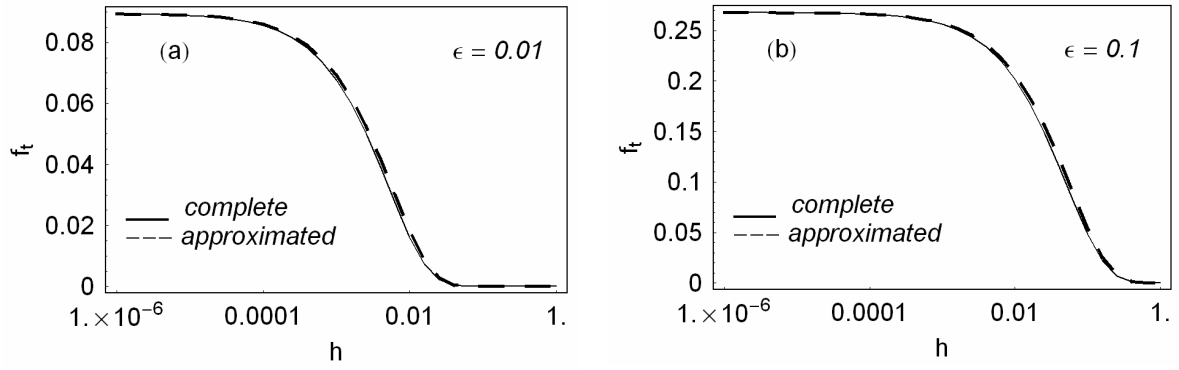


Figure 6: Variation of  $f_t$  with “ $h$ ” for fixed inverse aspect ratios  $\epsilon=0.01$  (a) and  $\epsilon=0.1$  (b), comparing the complete and approximated forms for  $E_{//c}$  employed in the  $f_t$  calculation.

It is observed in figures 4-6 that the approximated and complete forms for the trapped particle fraction agree reasonably well in all range of parameters representing large aspect ratio machines. We have made an extensive analysis for the error committed with the approximation (presented in details in Appendix 3), which is always below 20% for the parameter range of interest. We consider this error acceptable and for this reason the calculation of the trapped particle fraction for different launch points will be performed from now on in this paper using Eq.(16) over which is performed a poloidal average in order to obtain the total  $f_t$ .

It is also possible to generate profiles of trapped particle fraction for the full minor radius, as indicated in figure 7 for the same tokamak parameters as used for figure 3, but now with launch point averaging. Note that in the cases shown here, the trapped particle fraction is less than when a launch point at the outer midplane is considered (figure 3). It is also observed in figure 7(a) that when  $r/a=0.4$ , there is approximately 10% of error between the complete and approximated calculations. In this case  $\epsilon(r) \approx 0.11$ , and the value of  $h$  is roughly 0.1. We observe from figure A3.1(c) that our analysis for the error is consistent with this result. When the temperature rises, we expect the relative error between the two calculations to decrease. This is confirmed in figure 7(b).

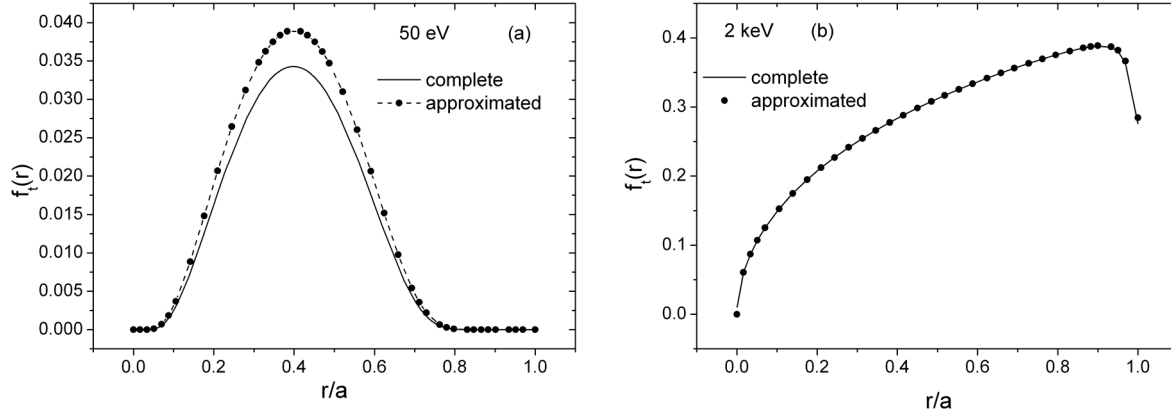


Figure 7: Comparison of the trapped particle fraction in the presence of the driven electric field for  $T_{e0} = 50 \text{ eV}$  (a), and  $T_{e0} = 2 \text{ keV}$  (b), obtained when the complete (eq.14) or approximated (eq.15) forms for  $E_{//c}$  are employed. In these cases launch point averaging is taken into account.

In the next section current density profiles are obtained for different central electron temperatures taking into account the detrapping effect of the toroidal electric field averaged over different poloidal launch points.

## 5. Current Density Profiles

The foregoing results can be used to develop profiles of current density in a typical tokamak, given a set of model assumptions such as those elaborated in section 3, but now replacing Eq.(6) for the trapped particle fraction by Eq. (16) in order to account for the average on different launch points.

The free parameters of the calculation are taken as listed in table 2, apart from the central temperature, which now assumes the values indicated in figures 8 and 9.

Figure 8 shows the current density profiles with electric field detrapping for different central electron temperatures. A fixed temperature profile peaking factor of  $\alpha_T = 2$  is considered here. In this case, as previously mentioned, the total plasma current is not the same in all cases as well as the safety factor profile. It is observed that as the temperature increases the effect of the electric field in detrapping particles is less pronounced, generating current density profiles more peaked in the central region. However, it should be emphasized that although the detrapping effect is diminished as the temperature increases, the cusp in the current density no longer exists since the trapped particle profile has a different behaviour due to the presence of the driven electric field. An alternative way of portraying the results, arguably of greater experimental relevance, is to adjust the profile parameter  $\alpha_T$  for each chosen value of central electron temperature, such that in addition to holding central  $q$  constant (at 1.0 in all the calculations so far), the edge  $q$  (equivalently the total current) is also

held constant. In figure 9, the value of  $\alpha_T$  has been adjusted to achieve an edge  $q$  of 5.51, which corresponds to the edge  $q$  value for  $T_{e0} = 2$  keV in figure 8.

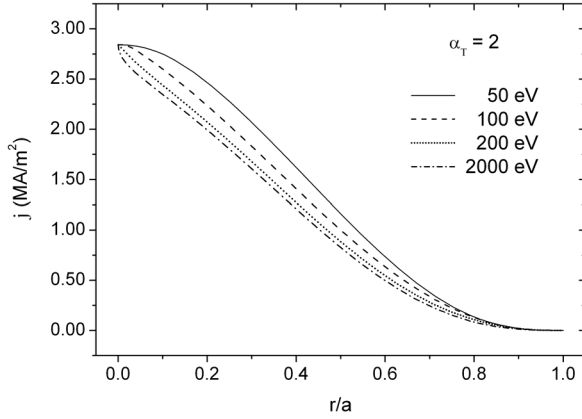


Figure 8: Current density profiles with electric field detrapping and constant temperature profile peaking factors  $\alpha_T = 2$ . The graphs are obtained for different central electron temperatures.

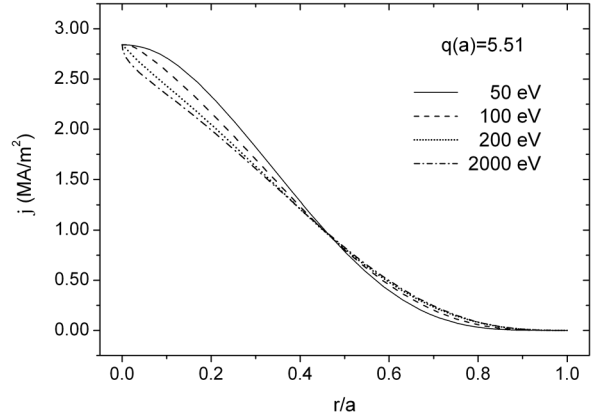


Figure 9: Current density profiles with electric field detrapping and constant edge  $q(a) = 5.51$ . The profiles are shown for different central electron temperatures as listed in the figure.

In the results shown in figures 8 and 9, if particles were assumed to be born at the outboard midplane, that is, not considering launch point average, the trapped particle fraction would be larger and the current density profiles would be below the curves shown in these figures. This behaviour is observed explicitly in figure 10.

In the next section collisionality effects will be evaluated and their role in detrapping particles will be convoluted with the electric field effect.

## 6. Collisionality effects

Appendix 4 develops the traditional convolution of neoclassical trapping with collisionality to account for the electric field detrapping effect. Since the collisionality parameter is defined as the ratio of effective collision frequency (for the scattering angle of interest) to the bounce frequency, it is also necessary to evaluate the modifications to the bounce frequency caused by the electric field. This is done in Appendix 5, where it is shown that the “tilting of the potential energy sine wave” exacerbates the usual (but usually neglected) non-linearity of the bounce oscillation, as well as reducing the bounce frequency at small amplitudes. The modified bounce period is given in Eq.(A5.2) by:

$$T_b(r) \approx 2.4\pi (1 - x(r)^2)^{-1/4} \sqrt{\frac{2}{\epsilon} \frac{R_0 q(r)}{v_{\perp}}},$$

and the collisionality parameter thus modified by the electric field is provided by Eq.(A4.10), obtained in Appendix 4:

$$v_{*e} \approx \sqrt{2} \times 1.2 \frac{R_0 q(r)}{v_{the}(r)} \varepsilon(r)^{-3/2} (1-x(r)^2)^{-1/4} \tau_{ee}^{-1},$$

with  $x(r)$  being given by  $x(r) = q(r) R_0 E_\phi / (\varepsilon E_\perp(r)_{(eV)})$  and  $\tau_{ee} = 3 (4\pi\varepsilon_0)^2 m_e^2 v_{the}^3 / (16 \sqrt{\pi} n_e e^4 \ln \Lambda)$ .

The current density profile, when collisionality effects are taken into account, is considered here according to the Hirshman et al. formulation given in ref.[9]:

$$j(r) = \sigma_{Spitzer} E_\phi \left( 1 - \frac{f_t(r)}{1 + \xi(Z_{eff})v_{*e}} \right) \left( 1 - \frac{c_R(Z_{eff})f_t(r)}{1 + \xi(Z_{eff})v_{*e}} \right). \quad (17)$$

All quantities in this expression are defined in Appendix 4. The trapped particle fraction used in this equation is now modified by the presence of the electric field, differently from the effect described in ref.[9]. In order to simplify our analysis but accounting for the launch point average contribution,  $f_t(r)$  is approximately considered here as given by 60% of the trapped particle fraction calculated for  $\theta=0$ . This approach is valid for most cases of interest in large aspect ratio machines within an error of about 15 to 25%. It is not valid, for instance, when there is a combination of high values of the normalised electric field (roughly larger than  $h > 0.01$ ) and small values of  $\varepsilon$ , which represents the region closer to the magnetic axis. In these cases, however, the trapped particle fraction is already nearly zero and the error committed is not so important. The following approach is thus considered for  $f_t$ :

$$f_t(r) \approx 0.6 \exp(-v(r)^2) \sqrt{\frac{2\varepsilon(r)}{1+2\varepsilon(r)}}, \quad (18)$$

with  $v(r) = \sqrt{E_{\perp c}(r)/T_e(r)}$  and  $E_{\perp c} = q(r) R_0 E_\phi / (\varepsilon(r) \times 0.7246)$ .

This results in the set of curves shown in figure 10, where all the usual parameters that vary in a tokamak minor radius profile have been taken as constants since only the central region is of interest in this case. Curves named as ‘‘conventional’’ in this plot are obtained by using the trapped particle fraction calculated only for launch points at the outer midplane (ie. without considering the launch point average, approximately accounted here by the factor 0.6), and without the correction to the bounce frequency in the collisional case. It can be seen that in every case where either the electric field or the collisionality effects are turned on, the derivative of the trapped particle fraction with respect to the inverse aspect ratio

vanishes at the minor axis, consistent with the analytical derivative of the simplified expression for the trapped particle fraction. Thus in reality there is never any “catastrophe” in the central current density in a tokamak. The parameters used for these calculations are as follows:  $E_\phi = 1$  V/m,  $q = 1$ ,  $R = 0.56$  m,  $T_{e0} = 200$  eV,  $n_{19} = 1$  and  $Z_{\text{eff}} = 1$ .

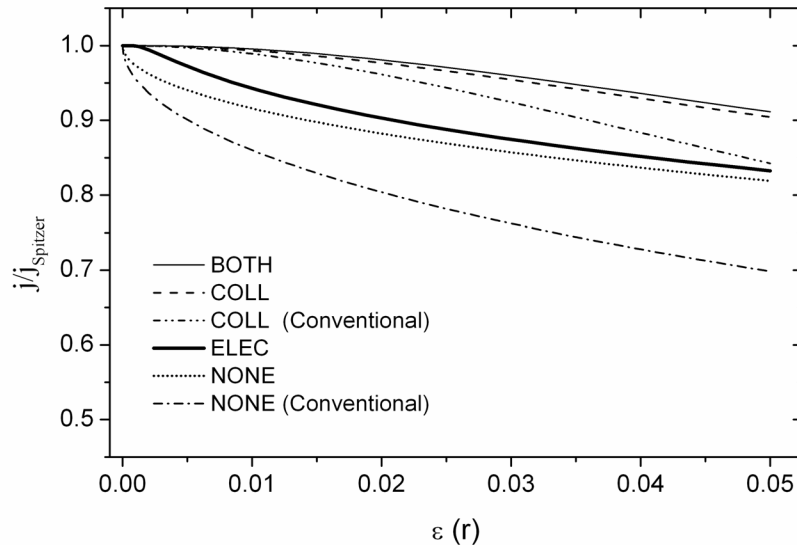


Figure 10: Normalised central current density with both collisionality and electric field terms, with one at a time, and with neither. The thicker full trace corresponds to the case where the electric field is considered alone. The “conventional” traces are obtained for  $f_i$  calculated for a launch point at the outer midplane (NONE) and without correction to the bounce frequency due to the presence of the electric field (COLL).

The conventional cusp in central neoclassical current density is clearly shown for reference, with either of the electric field or collisionality terms generating shoulders on the cusp so that the discontinuity is removed. For the parameters chosen, the collisionality term is clearly much stronger than that of the electric field. This situation can only be reversed in plasma conditions corresponding to tokamak start-up, when the toroidal electric field is very high and the density is very low (thus aggravating runaway electron production).

## 7. Conclusions

This work has extended the treatment of neoclassical resistivity in tokamaks to include a hitherto neglected term representing the parallel acceleration by the toroidal electric field acting to reduce the pitch angle of the electrons and hence the trapped particle fraction. In addition, new consideration has been given to averaging both the bounce frequency of the trapped particles and the trapping fraction with respect to the position of their birth (or launch) points distributed around the poloidal circumference. An analytic form for the electric field detrapping term has been developed, allowing it to be included in an approximate analytic expression for the overall neoclassical current density. This can be readily

differentiated with respect to inverse aspect ratio to demonstrate that there is never any real “neoclassical catastrophe” at the minor axis of a tokamak. Analyses with typical tokamak conditions show that the collisionality term dominates the detrapping effects except in extreme start-up conditions with high electric field and low plasma density. Even in normal tokamak discharge conditions, some of the corrections developed above to bounce frequency and flux-surface averaged trapped particle fraction as well as the concept of a toroidal force detrapping a section of the particle population will be significant. They could be expected to modify the behaviour of a variety of neoclassical phenomena such as bootstrap current, potato or kidney-bean orbits, neoclassical tearing modes and certain types of momentum and current drive relying on inter-species drag.

## 8. References

- [1] – Hinton F. L. and Hazeltine R. D., 1976 *Rev. Mod. Physics* **48**, 239.
- [2] - Hirshman S.P, Sigmar, D. J., 1981 *Nuclear Fusion* **21**, 1079.
- [3] - Bickerton R. J., Connor J. W., Taylor J. B., 1971 *Nature Phys. Science* **229**, 110.
- [4] - Carrera R., Hazeltine R. D., and Kotschenreuther M., 1986 *Phys. Fluids* **29**, 899.
- [5] - Helander P., 2000 *Phys. Plasmas* **7**, 2878.
- [6] - Wang S., 1998 *Phys. Plasmas* **5**, 3319.
- [7] - Chu T. K., 1996 *Phys. Plasmas* **3**, 3397.
- [8] - Wesson J., in *Tokamaks*, 2nd Edition, (Oxford University Press (1997)), p.128.
- [9] - Hirshman S. P., Hawryluk R. J. and Birge B., 1977 *Nuclear Fusion* **17**, 611.
- [10] - Hinton F. L. and Rosenbluth M. N., 1973 *Phys. of Fluids* **16**, 836.

## 9. Appendices

### Appendix 1

Mono-energetic particles launched at the outboard midplane

### Appendix 2

Integration of the trapped particle fraction over the velocity distribution, with finite toroidal electric field and launch points at the outer midplane.

### Appendix 3

Launch point averaging of trapped particle fraction, with finite toroidal electric field

### Appendix 4

Neoclassical collisionality in the presence of a toroidal electric field

### Appendix 5

Bounce frequency in the presence of a toroidal electric field

## Appendix 1

### Mono-energetic particles launched at the outboard midplane

The magnetic (mirror) force on a charged particle along the magnetic field in a circular plasma of large aspect ratio geometry is given by

$$\begin{aligned}
 F_m &= E_{\perp}/B \nabla B (B_{\theta}/B_{\phi}) \text{Sin}\theta \\
 &= E_{\perp} (1 + \varepsilon) (B_{\theta}/B_{\phi}) \text{Sin}\theta / \left[ R_0 (1 + \varepsilon \text{Cos}\theta)^2 \right] \\
 \therefore \\
 F_m &= E_{\perp} \left[ \frac{(1 + \varepsilon)}{R_0 (1 + \varepsilon \text{Cos}\theta)^2} \right] \frac{\varepsilon}{q} \text{Sin}\theta \quad ,
 \end{aligned}$$

where the  $B_{\theta}/B_{\phi}$  term (the ratio between the poloidal and toroidal magnetic fields), represents the component of the  $\nabla B$  force along the magnetic field line, and the  $\text{Sin}\theta$  term accounts for the modulation in poloidal angle (since the flux surface is orthogonal to the  $\nabla B$  force at the inboard and outboard midplane). In the equation above, the ratio  $\mu = E_{\perp}/B$  is constant and evaluated in the midplane, where the magnetic field assumes its minimum value given, in the large aspect ratio approach, by  $B = B_0/(1 + \varepsilon)$ . It is also considered to this order that  $\nabla B = B_0 R_0 / R^2$  and that the safety factor  $q$  is described as  $q = r B_{\phi} / (R_0 B_{\theta})$ , with  $R_0$  being the major tokamak radius.

The electrostatic acceleration force on the particle is given by

$$F_e = -e E_{\phi} = -e V_{\text{loop}} / (2 \pi R_0 (1 + \varepsilon \text{Cos}\theta))$$

(under the ordering assumption  $B_{\theta} \ll B_{\phi}$ ).

The sum of the two forces is accordingly

$$F = E_{\perp} \left[ \frac{(1 + \varepsilon)}{R_0 (1 + \varepsilon \text{Cos}\theta)^2} \right] \frac{\varepsilon}{q} \text{Sin}\theta - e E_{\phi} \quad ,$$

where the poloidal angle  $\theta$  can be replaced by  $\ell/(qR_0)$ , with  $\ell$  representing the length along a field line. The integration of this force along  $\ell$ , yields an expression to the parallel energy added by the electric field given by:

$$\int_0^{\ell} F d\ell = \delta E_{//}(\ell) = E_{\perp} \varepsilon \frac{\left[ 1 - \text{Cos}\left(\frac{\ell}{qR_0}\right) \right]}{1 + \varepsilon \text{Cos}\left(\frac{\ell}{qR_0}\right)} - e E_{\phi} \ell \quad .$$

Substituting the toroidal angle  $\phi$  for  $\ell/R_0$  and multiplying the second right hand term by  $q/q$  to achieve the variable  $\phi/q$  (the poloidal angle  $\theta$ ), the parallel potential energy can be finally written as:

$$\delta E_{//}(\phi) = E_{\perp} \varepsilon \frac{\left[1 - \text{Cos}\left(\frac{\phi}{q}\right)\right]}{1 + \varepsilon \text{Cos}\left(\frac{\phi}{q}\right)} - eE_{\phi} q R_0 \frac{\phi}{q} . \quad (\text{A1.1})$$

The shape of the potential energy curve is thus a tilted sine wave. If the initial parallel energy of a launched particle, plus that gained from the electric field, is enough to overcome the potential energy hill, the particle will not be trapped in the magnetic mirror. The peak of this function is found for the angle which is a solution of the following equation:

$$\frac{\text{Sin}(\phi/q)}{[1 + \varepsilon \text{Cos}(\phi/q)]^2} = \frac{qeE_{\phi} R_0}{\varepsilon E_{\perp} (1 + \varepsilon)},$$

Note that when the electric field  $E_{\phi} = 0$ , this peak corresponds to the solution  $\text{Sin}(\phi/q) = 0$ . The point of maximum is obtained for  $(\phi/q) = \pi$ ; that is when  $\text{Cos}(\phi/q) = -1$ . Substituting this back into the equation for  $\delta E_{//}(\phi)$  in A1.1, for a zero electric field, the parallel critical energy results as given below:

$$E_{//c} = E_{\perp} \frac{2\varepsilon}{(1 - \varepsilon)},$$

which is consistent with the well known critical energy found when the driven electric field is not taken into account [8]. Having checked this, and in order to simplify the calculations and analyses throughout this paper, the correction in  $\varepsilon$  in the denominator of the first term of Eq.(A1.1) will be neglected from now on. The parallel potential energy is thus written as:

$$\delta E_{//}(\phi) = E_{\perp} \varepsilon \left[1 - \text{Cos}\left(\frac{\phi}{q}\right)\right] - qeE_{\phi} R_0 \frac{\phi}{q} \quad (\text{A1.2})$$

and the critical parallel energy is now obtained, at this approximation, for:

$$\text{Sin}(\phi/q) = qeE_{\phi} R_0 / (\varepsilon E_{\perp}) = x, \text{ say.} \quad (\text{A1.3})$$

Thus

$$\text{Cos}(\phi/q) = \pm \sqrt{1 - x^2} .$$

Substituting now this back into the equation A1.2, and noting that it is the value of  $\phi/q$  just below  $\pi$  which represents the peak, the parallel critical energy is then obtained as:

$$E_{//c} = E_{\perp} \varepsilon \left[ 1 + \sqrt{1 - x^2} - x (\pi - \arcsin(x)) \right], \quad (\text{A1.4})$$

where the surd takes the positive sign in order to recover the usual form,  $E_{//c}/E_{\perp} = 2\varepsilon$ , for the critical parallel energy when  $x = 0$  in the approximation adopted above.  $E_{//c}$  is the minimum value of  $E_{//}$  necessary for a particle launched at that  $E_{//}$ , from  $\theta = 0$ , to overcome the potential energy barrier, for a given value of  $x$  (which characterises the strength of the parallel electric field).

If  $x$  is sufficiently large, the potential energy curve has a point of inflexion, that is the electrostatic and magnetic forces balance each-other. This represents a “no trapped particles” threshold, which as shown in figure 1 occurs when  $x = 1$ , ie.

$$\frac{E_{\perp} \varepsilon}{R_0 q} \leq \frac{e V_{\text{loop}}}{2\pi R_0} \quad (\text{A1.5})$$

ie when 
$$V_{\text{loop}} \geq \frac{2\pi \varepsilon E_{\perp}}{q},$$
 with energies expressed in eV.

When the first peak is at the same potential energy as the launch point, particles launched with zero parallel energy will not be trapped. The worst case corresponds to the parallel launch energy being zero, since any oppositely launched particle will reflect “upstream”, where the magnetic and electrostatic forces act in the same direction, sending the particle back through the launch point (ignoring the half-banana-orbit width, negligible for electrons).

The critical toroidal electric field for particles launched from the outboard midplane ( $\theta = 0$ ) with no parallel velocity is given by solving the expression for  $E_{//c} = 0$ , with the result:

$$E_{\phi} \geq 0.7246 \varepsilon E_{\perp} / (e q R_0),$$

or 
$$V_{\text{loop}} \geq 1.4492\pi \varepsilon E_{\perp} / q \quad (\text{with } E_{\perp} \text{ in eV}).$$

For a given electric field, this can be rearranged to yield a critical perpendicular energy (at which the electric field accelerates the launched particles sufficiently to detrap them, whatever the initial  $v_{//}$ ), below which no particles launched at the outboard midplane are trapped:

$$E_{\perp c} \leq E_{\phi} e q R_0 / (0.7246 \varepsilon).$$

Trapped particles occupy a region in the velocity space delimited by curves shown with full lines, in figure 2, for three chosen values of  $v_{\perp c}$ . For a given value of the perpendicular velocity, particles will be trapped within a range of parallel velocities between the values  $\pm v_{//c}$ .

## Appendix 2

### Integration of the trapped particle fraction over the velocity distribution, with finite toroidal electric field and launch points at the outer midplane

This is here achieved using cylindrical coordinates in velocity space, represented by the parallel and perpendicular components of the particle velocity, with the trapped particle fraction given as:

$$f_t(r) = \int_{v_{\perp c}}^{\infty} \int_{-v_{//c}}^{v_{//c}} 2\pi f(v) v_{\perp} dv_{//} dv_{\perp} \quad , \quad (A2.1)$$

or substituting  $f(v)$  by a Maxwellian distribution function,

$$f_t(r) = \int_{v_{\perp c}}^{\infty} \int_{-v_{//c}}^{v_{//c}} 2\pi \left(\frac{m}{2\pi T}\right)^{3/2} \exp[-(v_{//}^2 + v_{\perp}^2)/v_{th}^2] v_{\perp} dv_{//} dv_{\perp} \quad .$$

The previous equation can be rearranged as:

$$f_t(r) = 4\pi \left(\frac{m}{2\pi T}\right)^{3/2} \int_{v_{\perp c}}^{\infty} v_{\perp} \exp[-(v_{\perp}^2/v_{th}^2)] \int_0^{v_{//c}} \exp[-v_{//}^2/v_{th}^2] dv_{//} dv_{\perp} \quad ,$$

which yields the following result after performing the integration over the parallel velocity:

$$f_t(r) = \left(\frac{m}{T}\right) \int_{v_{\perp c}}^{\infty} v_{\perp} \exp[-(v_{\perp}^2/v_{th}^2)] \operatorname{Erf}\left(\frac{v_{//c}(r, v_{\perp})}{v_{th}}\right) dv_{\perp} \quad . \quad (A2.2)$$

In Eq. (A2.2), Erf is the error function and  $v_{//c}(r, v_{\perp})$  is taken from the expression of  $E_{//c}$  given by Eq.(5).

This reduces to the usual large aspect ratio trapped particle fraction when the normalised electric field ( $x$ ) is zero. Taking the expression for  $E_{//c}/E_{\perp}$  in the case  $x=0$ , resulting when the full expression for the parallel potential energy, given by Eq.(A1.1), is considered, it is possible to write:

$$\frac{E_{//c}}{E_{\perp}} = \left( \frac{2\varepsilon}{1-\varepsilon} \right) \Rightarrow \frac{v_{//c}}{v_{\perp}} = \sqrt{\frac{2\varepsilon}{1-\varepsilon}} \quad \text{and} \quad v_{\perp c} = 0 \quad (x=0).$$

In these expressions, the dependence of  $v_{//c}$  on  $r$  and  $v_{\perp}$  was dropped in order to simplify the notation. Substituting this into (A2.2) we get:

$$f_t(r) = \left( \frac{m}{T} \right) \int_0^{\infty} v_{\perp} \exp[-(v_{\perp}^2/v_{th}^2)] \operatorname{Erf} \left( \frac{\sqrt{\frac{2\varepsilon}{1-\varepsilon}} v_{\perp}}{v_{th}} \right) dv_{\perp}$$

$$f_t(r) = \left( \frac{m}{T} \right) \frac{\sqrt{\frac{\varepsilon}{2-2\varepsilon}} v_{th}^2}{\sqrt{(1+\varepsilon)} \sqrt{1-\varepsilon}} \Rightarrow f_t(r) = \sqrt{\frac{2\varepsilon}{1+\varepsilon}}.$$

In order to compute the integral given in (A2.2) in the general case, when the acceleration effect of the electric field is taken into account, it has been introduced a change of variables to the normalised perpendicular velocity so that  $y = v_{\perp}/v_{th}$ . Noting that  $v_{th} = \sqrt{2T/m}$ , Eq.(A2.2) assumes then the following form:

$$f_t(r) = 2 \int_{v_{\perp c}/v_{th}}^{\infty} y \exp[-y^2] \operatorname{Erf} \left( \frac{v_{//c}(r, y)}{v_{th}(r)} \right) dy. \quad (\text{A2.3})$$

We consider now the relation between  $v_{//c}$  and  $v_{\perp}$  given by Eq.(5), which neglects the correction in  $\varepsilon$  in the denominator of the first term of the parallel potential energy (Eq.(A1.1)), and rewrite it in terms of this new variable  $y$ :

$$\frac{v_{//c}(r, y)}{v_{th}(r)} = \sqrt{2\varepsilon} y \left( 1 - \frac{v_{\perp c}^2(r)}{y^2 v_{th}^2(r)} \right)^{1/2}. \quad (\text{A2.4})$$

Substituting Eq.(A2.4), into Eq.(A2.3) the following equation is provided for the trapped particle fraction:

$$f_t(r) = 2 \int_{v(r)}^{\infty} y \exp[-y^2] \operatorname{Erf} \left( \sqrt{2\varepsilon} \left( y^2 - v(r)^2 \right)^{1/2} \right) dy, \quad (\text{A2.5})$$

where  $v(r) = \sqrt{E_{\perp c}(r)/T_e(r)} = v_{\perp c}(r)/v_{th}(r)$ .

The integration by parts of Eq.(A2.5) yields the result below:

$$f_t(r) = -\exp(-y^2) \operatorname{Erf}\left(\sqrt{2\varepsilon} \left(y^2 - v(r)^2\right)^{1/2}\right) \Big|_{v(r)}^{\infty} + \int_{v(r)}^{\infty} \exp(-y^2) \frac{\partial \operatorname{Erf}\left(\sqrt{2\varepsilon} \left(y^2 - v(r)^2\right)^{1/2}\right)}{\partial y} dy \quad , \quad (\text{A2.6})$$

where the first term goes to zero since  $\operatorname{Erf}[\infty]=1$  and  $\operatorname{Erf}[0]=0$ . In the second term, let us call  $\partial \operatorname{Erf}/\partial y$  as  $\operatorname{Erf}'[f[y]]$ . The derivative of the Error Function given in (A2.6) can be written as:

$$\operatorname{Erf}'\left(\sqrt{2\varepsilon} \left(y^2 - v(r)^2\right)^{1/2}\right) = \frac{4 \varepsilon(r) y}{\sqrt{\pi}} \frac{\exp\left[-2\varepsilon(r) \left(y^2 - v(r)^2\right)\right]}{\sqrt{2\varepsilon(r) \left(y^2 - v(r)^2\right)}} \quad , \quad (\text{A2.7})$$

which is substituted into Eq.(A2.6) leading to:

$$f_t(r) = \int_{v(r)}^{\infty} \exp(-y^2) \frac{4 \varepsilon(r) y}{\sqrt{\pi}} \frac{\exp\left(-2\varepsilon(r) \left(y^2 - v(r)^2\right)\right)}{\sqrt{2\varepsilon(r) \left(y^2 - v(r)^2\right)}} dy \quad (\text{A2.8})$$

A new change of variables such as  $z = \sqrt{2\varepsilon(r) \left(y^2 - v(r)^2\right)}$ , allows an analytical solution to the integral in (A2.8), generating the following expression for the trapped particle fraction when a launch point at the outer midplane is considered:

$$f_t(r) = \exp(-v(r)^2) \sqrt{\frac{2\varepsilon(r)}{1+2\varepsilon(r)}} \quad . \quad (\text{A2.9})$$

### Appendix 3

#### Launch point averaging of trapped particle fraction, with finite toroidal electric field

As pointed out in section 4, in order to derive the potential energy function for a particle under the action of the driven electric field, one has to have in mind that the minimum of the potential energy is not at the outboard midplane, but is shifted downstream by the toroidal electric field (oppositely for ions and electrons as already mentioned), as can be observed in figure 1, section 2. The minimum of the potential energy curve occurs at the other force-balance root (ie the other root of the equation provided when the derivative of the potential energy curve, (Eq.(A1.2)), equals 0). This minimum is given by:

$$E_{//\min} = E_{\perp} \varepsilon \left[ 1 - \sqrt{1 - x^2} - x \arcsin(x) \right] \quad (\text{A3.1})$$

The required root here is no longer at  $\pi - \arcsin(x)$  but simply  $\arcsin(x)$ , and the surd now has to have the negative sign to recover  $E_{//} = 0$  when  $x = 0$ . Clearly  $x$  has to be less than 1.0 for this to remain valid and  $x = 1$  corresponds to the condition of “no trapped particles” threshold when the potential energy well marginally disappears. This condition is described by Eq. (A1.5). When  $x > 1$ , there are no trapped particles. We note that:

$$x = \text{Sin}(\phi/q) = \text{Sin}\theta \quad (\text{A3.2})$$

where  $\theta$  is the poloidal angle, so  $\theta = \text{Sin}^{-1}(x)$  defines the launch point with the minimum potential energy. It would seem natural to choose a set of launch points starting from this value of  $\theta$ , but this is impracticable since this value of  $\theta$  depends upon  $E_{\perp}$  which is a key variable in the velocity space integral carried out for each launch point. (One could average over launch points for each velocity, but not over velocity for each launch point.)

For each launch point, we need to know the starting potential energy  $E_{//0}(\theta)$ , given by selecting a value for  $\theta (= \phi/q)$ , in the equation for  $\delta E_{//}(\phi)$  given in Eq.(1);

$$E_{//0}(\theta) = E_{\perp} \varepsilon [1 - \text{Cos}(\theta)] - qeE_{\phi} R_0 \theta \quad (\text{A3.3})$$

Whatever the launch combination of  $E_{\perp}$  and  $E_{//}$ , particles are accelerated by the electric field towards the point of maximum potential energy ( $\text{PE}_{\max}$ ), which remains given by the expression previously identified with  $E_{//c}$ :

$$PE_{\max} = E_{\perp} \varepsilon \left[ 1 + \sqrt{1 - x^2} - x (\pi - \arcsin(x)) \right] \quad (\text{A3.4})$$

The revised  $E_{//c}$  is this expression corrected by the potential energy  $E_{//0}(\theta)$  at the selected launch point  $\theta$ , thus

$$E_{//c}(\theta) = PE_{\max} - E_{//0}(\theta) \quad . \quad (\text{A3.5})$$

As before, any particle launched with  $E_{//}$  larger than this  $E_{//c}$  will be detrapped by the toroidal electric field, so for a given  $E_{\perp}$ , the trapped particle fraction for the respective local temperature can be calculated as before.

Thus we are now ready to extend the calculation to account for the full range of poloidal angles of launch point around each flux surface, including the corrections to the potential energy curve for the shift of the potential energy minimum due to the electric field. Substituting Eqs.(A3.3) and (A3.4) into (A3.5), the following equation results for  $E_{//c}(\theta)$ :

$$E_{//c}(\theta) = E_{\perp} \varepsilon \left( 1 + \sqrt{1 - x^2} - x (\pi - \arcsin(x)) - 1 + \text{Cos}(\theta) + x\theta \right) \quad (\text{A3.6})$$

where as before,  $x = qeE_{\phi}R_0/(\varepsilon E_{\perp})$ .

Similarly to the derivation in Appendix 2 (Eq.A2.3), the expression for the trapped particle fraction related to a given launch point  $\theta$  is now given by:

$$f_t(r, \theta) = 2 \int_{v(r, \theta)}^{\infty} y \exp[-y^2] \text{Erf} \left( \frac{v_{//c}(r, \theta, y)}{v_{th}} \right) dy \quad (\text{A3.7})$$

where  $y = v_{\perp}/v_{th}$  and  $v(r, \theta) = \sqrt{E_{\perp c}(r, \theta)/T_e(r)} = v_{\perp c}(r, \theta)/v_{th}(r)$  . (A3.8)

The expression for  $v_{//c}/v_{th}$  in the error function given in (A3.7) is taken from Eq.(A3.6) for which we propose an approximation in order that the integral in  $f_t(r)$  may be obtained analytically. Accordingly, we will let

$$f(x, \theta) = \left( 1 + \sqrt{1 - x^2} - x (\pi - \arcsin(x)) - 1 + \text{Cos}(\theta) + x\theta \right) \quad (\text{A3.9})$$

and write an approximated form to it given by:

$$f_s(x, \theta) = f(0, \theta) - f(0, \theta) \frac{x}{x_c(\theta)} \quad (\text{A3.10})$$

In this way, Eq.(A3.6) becomes:

$$E_{//c}(\theta) = E_{\perp} \varepsilon \left[ f(0, \theta) - f(0, \theta) \frac{x}{x_c(\theta)} \right] \quad (\text{A3.11})$$

or in terms of velocities:

$$\frac{v_{//c}(r, \theta, y)}{v_{th}(r)} = \sqrt{\varepsilon(r) (1 + \cos(\theta))} \left[ y^2 - \frac{v_{\perp c}^2(r, \theta)}{v_{th}^2(r)} \right]^{1/2}, \quad (\text{A3.12})$$

where we have used the fact that the ratio  $x/x_c$  can be written as  $E_{\perp c}/E_{\perp}$  and applied the change of variables given by  $y = v_{\perp}/v_{th}$ . We have also substituted  $f(0, \theta) = 1 + \cos \theta$ .

Introducing the result (A3.12) into (A3.7), the integral that provides  $f_t(r, \theta)$  can be obtained analytically, similarly to the case of  $\theta = 0$  (Appendix 2). In this way, the trapped particle fraction related to a given launch point results as follows:

$$f_t(r, \theta) = \exp(-v(r, \theta)^2) \frac{\sqrt{\varepsilon(r) (1 + \cos \theta)}}{\sqrt{1 + \varepsilon(r) (1 + \cos \theta)}}, \quad (\text{A3.13})$$

with  $v(r, \theta)$  already defined in (A3.8).

The total trapped particle fraction averaged over several launch points will be finally given by:

$$f_t(r) = \frac{1}{2\pi} \int_{-\pi}^{\pi} f_t(r, \theta) d\theta \quad (\text{A3.14})$$

We have analysed the approximation represented by equation (A3.11) in a large range of tokamak parameters in order to check its accuracy. In order to describe this analysis here let us rewrite Eq.(A3.6) in terms of velocities and substitute  $x$  by  $x = g(r)/E_{\perp}$ , where  $g(r)$  is given by  $g(r) = q(r) E_{\phi} R_0 / \varepsilon(r)$ . This function can still be redefined as:

$$g(r) = \frac{q(r) V_{loop}}{2\pi \varepsilon(r)}, \quad (\text{A3.15})$$

with  $x$  assuming the form:

$$x = \frac{h(r)}{\varepsilon(r) y^2}, \quad \text{where } h(r) = \frac{q(r) V_{loop}}{2\pi T e(r)}. \quad (\text{A3.16})$$

In Eq. (A3.16) we have used again the change of variables  $y = v_{\perp}/v_{th}$  from where we get  $E_{\perp} = y^2 Te$ . In this way, Eq.(A3.6) is rearranged, as given below, in terms of general variables embedded in this new function  $h(r)$  that allows an analysis for the accuracy of the approximation represented by Eq. (A3.11), for large aspect ratio machines:

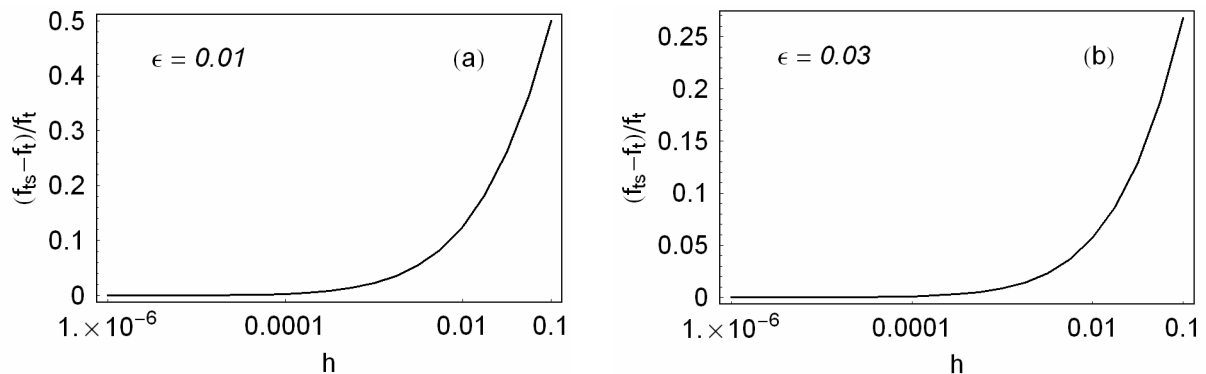
$$\frac{v_{//c}(r, \theta, y)}{v_{th}} = y \left\{ \epsilon \left[ 1 + \sqrt{1 - \frac{h(r)^2}{\epsilon^2 y^4}} - \frac{h(r)}{\epsilon y^2} \left( \pi - \arcsin\left(\frac{h(r)}{\epsilon y^2}\right) \right) - 1 + \cos\theta + \frac{h(r)}{\epsilon y^2} \theta \right] \right\}^{1/2}. \quad (A3.17)$$

The function  $h(r)$ , similarly to  $x$ , represents the normalised electric field strength.

Considering typical values of tokamak parameters,  $h(r)$  is allowed to range from  $1 \times 10^{-6}$  to 1, and plots of  $f_t$  are shown both for some fixed values of  $\epsilon$  or fixed values of  $h$ , as in figures 4-6, in section 4.

The relative errors  $((f_{ts}-f_t)/f_t)$ , between the complete and approximated forms, for some fixed values of  $\epsilon$ , such as  $\epsilon = 0.01, 0.03, 0.1$  and  $0.5$  are shown in figure A3.1. The value  $\epsilon = r/R_0 = 0.5$  is considered here as our limit for large aspect ratio tokamaks. In the case of  $\epsilon = 0.1$ ,  $h$  is shown to range up to 0.1 and 1, respectively represented by figures A3.1(c) and A3.1(d). However, values of  $h$  higher than 0.1, are not generally of relevance in typical tokamak machines.

We can see from these figures that the relative error between the complete and approximated calculations for  $h$  up to  $h=0.1$  remains below 25 or 30%. The highest errors are obtained when  $h \approx 1 \times 10^{-1}$  and for low values of  $\epsilon$ . However, in these cases, the trapped particle fraction is very small and the error we may commit between the two calculations is not important. This can be confirmed in figures 4(b) and 5(b) in section 4. We observe that when  $h \approx 1 \times 10^{-1}$  and  $\epsilon = 0.01$  or  $\epsilon = 0.03$ , which corresponds to errors of about 50 to 25% between the two calculations, (figures A3.1(a) and A3.1(b)), the trapped particle fraction is already nearly zero as shown in figure 5(b).



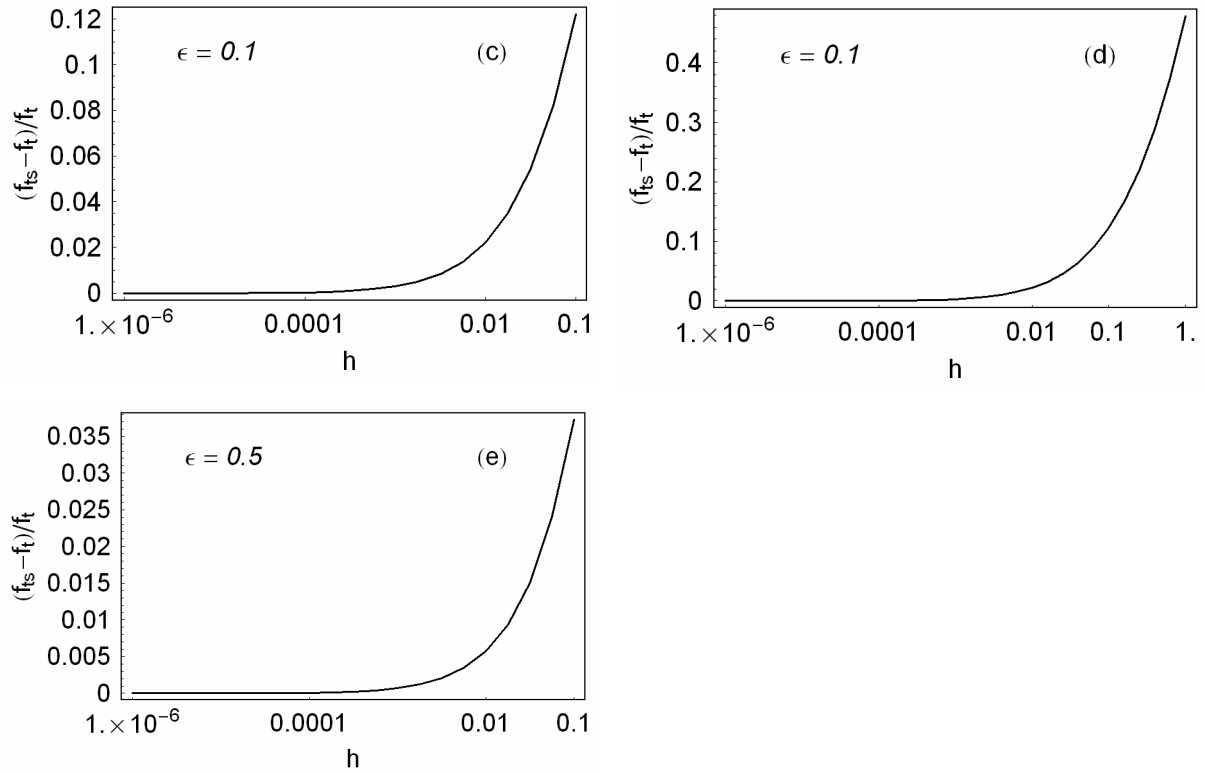


Figure A3.1: Relative errors between the approximated and complete calculations for  $f_i$  against “ $h$ ” and for fixed values of the inverse aspect ratio  $\epsilon$ .

So, we can conclude that the trapped particle fraction obtained from an approximated calculation that results in Eq.(A3.13) provides relative errors, when compared to the exact calculation, always below 20% for the parameter range of interest, which is considered acceptable in the scope of this paper. It should be also emphasised that absolute errors, given only by the difference between the complete and approximated forms, will be always less than the relative errors presented here. The errors obtained when  $h \rightarrow 0.1$ , which represent the largest deviations introduced by the approximated form in relation to the complete calculation, assume these high values since the denominator  $f_t$  in the error estimate is always small for such values of  $h$ .

## Appendix 4

### Neoclassical collisionality in the presence of a toroidal electric field

The neoclassical conductivity allowing for collisionality (but traditionally neglecting parallel electric field) can be approximated by an analytical formula proposed in [9] as:

$$\frac{\sigma_{\text{NC}}}{\sigma_0} = \Lambda_E(Z_{\text{eff}}) \left( 1 - \frac{f_t(r)}{1 + \xi(Z_{\text{eff}})v_{*e}} \right) \left( 1 - \frac{c_R(Z_{\text{eff}})f_t(r)}{1 + \xi(Z_{\text{eff}})v_{*e}} \right) \quad (\text{A4.1})$$

where  $\sigma_0 \Lambda_E(Z_{\text{eff}})$  is the Spitzer conductivity corrected for impurities and defined in Eq.(9);  $v_{*e} = v_{\text{eff}}/\omega_b$  is the collisionality parameter (ie. the ratio of the effective collision frequency for detrapping to the bounce frequency of the trapped particles) and

$$Z_{\text{eff}} = \sum_{i \neq e} \frac{n_i Z_i^2}{n_e}, \quad (\text{A4.2})$$

$$\Lambda_E(Z_{\text{eff}}) = \frac{3.40}{Z_{\text{eff}}} \left( \frac{1.13 + Z_{\text{eff}}}{2.67 + Z_{\text{eff}}} \right), \quad (\text{A4.3})$$

$$c_R(Z_{\text{eff}}) = \frac{0.56}{Z_{\text{eff}}} \left( \frac{3.0 - Z_{\text{eff}}}{3.0 + Z_{\text{eff}}} \right), \quad (\text{A4.4})$$

$$\xi(Z_{\text{eff}}) = 0.58 + 0.20 Z_{\text{eff}}. \quad (\text{A4.5})$$

The classical collision frequency  $\nu_c$  is usually defined for a scattering angle of one radian (sometimes 90°) developed in a random-walk diffusive process by integration over a large number of Coulomb collisions, each producing very tiny modifications to the pitch angle. Accordingly, the effective collision frequency is given by the one-radian collision frequency divided by the square of the scattering angle of interest, which is now the order of  $\sqrt{2\varepsilon}$ , thus:

$$\nu_{\text{eff}} \approx \frac{\nu_c}{2\varepsilon} \quad (\text{A4.6})$$

Let us introduce here the collisionality parameter ( $v_{*e} = v_{\text{eff}}/\omega_b$ ), following the formalism described in refs. [9,10] as:

$$v_{*e} = \frac{\sqrt{2} v_{ee} R_0 q}{\epsilon^{3/2} v_{\text{the}}} , \quad (\text{A4.7})$$

chosen independent of  $Z_{\text{eff}}$ . The thermal velocity  $v_{\text{the}}$  is defined here as  $v_{\text{the}} = \sqrt{2T_e/m}$  and  $\tau_{ee} = v_{ee}^{-1}$  is given by:

$$\tau_{ee} = \frac{3}{16 \sqrt{\pi}} (4\pi\epsilon_0)^2 \frac{m_e^2 v_{\text{the}}^3}{n_e e^4 \ln \Lambda} . \quad (\text{A4.8})$$

The bounce frequency obtained when the action of the electric field is not considered, is given according to Eq. (A5.1) in Appendix 5 as:

$$\omega_b = \sqrt{\frac{\epsilon}{2}} \frac{v_{\perp}}{q R_0} = \epsilon^{1/2} \frac{v_{\text{th}}}{q R_0}$$

where it has been considered that  $v_{\perp} = \sqrt{2} v_{\text{th}}$ .

Equation A4.7 will now be developed to account for the introduction of the parallel electric field, which modifies  $\omega_b$  and hence  $v_{*e}$ , as well as directly modifying  $f_i$ . As derived in Appendix 5, the bounce period allowing for the electric field is given by Eq.(A5.2):

$$T_b(r) \approx 2.4\pi (1-x(r)^2)^{-1/4} \sqrt{\frac{2}{\epsilon}} \frac{R_0 q(r)}{v_{\perp}} ,$$

and the bounce frequency in terms of the thermal velocity is thus written as:

$$\omega_b = \frac{2\pi}{T_b(r)} \approx \frac{1}{1.2} \frac{v_{\text{th}}}{R_0 q} \sqrt{\epsilon} (1-x(r)^2)^{1/4} . \quad (\text{A4.9})$$

Taking into account the expression for the bounce frequency when there is no electric field, the collisionality parameter in Eq.(A4.7) will be modified by the new  $\omega_b$  given above, according to:

$$v_{*e} \approx \sqrt{2} \times 1.2 \frac{R_0 q(r)}{v_{the}} \varepsilon^{-3/2} (1 - x(r)^2)^{-1/4} \tau_{ee}^{-1} , \quad (\text{A4.10})$$

where  $x(r)$  is described by:

$$x(r) = \frac{q(r) R_0 E_\phi}{\varepsilon E_\perp(r)(\text{eV})} . \quad (\text{A4.11})$$

Here  $E_\perp$  is taken as  $E_\perp(\text{eV}) \approx m_e v_{the}^2 / e$  and instead of defining a value of  $x$  for each particle, an average value of  $x$  is implied, using the mean thermal velocity of the electron population as  $E_\perp$ .

A set of curves showing the ratio of the current density profile to its Spitzer value is shown in figure 10 with all plasma profile parameters kept constant since we are interested in analysing only the central plasma region. In order to compute these profiles, the following procedure is adopted: it has been considered that if the variable  $x(r)$ , given by Eq.(A4.11), results below unity, then the collisionality parameter  $v_{*e}$  is calculated through Eq.(A4.10); otherwise we consider that all particles would be untrapped, ie.  $f_i(r)=0$ , reducing to the classical case where the current density is given by its Spitzer value. The trapped particle fraction is evaluated using Eq.(18) accounting for the 0.6 multiplying factor as an approach to the launch point average calculation. The parameters used in these calculations are, as already listed in section 6, the following:  $E_\phi = 1 \text{ V/m}$ ,  $q = 1$ ,  $R = 0.56 \text{ m}$ ,  $T_{e0} = 200 \text{ eV}$ ,  $n_{i9} = 1$  and  $Z_{\text{eff}} = 1$ .

## Appendix 5 Bounce frequency in the presence of a toroidal electric field

The trapped particle bounce frequency is generally derived as a simple harmonic motion (SHM) in the toroidal direction, given the magnetic gradient force described at the beginning of Appendix 1;

$$\partial^2 S / \partial t^2 = -\omega^2 S ,$$

$$R_0 \frac{\partial^2 \phi}{\partial t^2} = -E_\perp \left[ \frac{(1 + \varepsilon)}{R_0 (1 + \varepsilon \text{Cos}\theta)^2} \right] \frac{\varepsilon}{qm} \text{Sin}\theta ,$$

where  $S = R_0 \phi$  and  $m$  is the mass of a particle. For small angle excursions such as  $\text{Sin}\theta \sim \theta = \phi/q$ , and for  $\varepsilon \ll 1$ , this expression can be reduced to:

$$\frac{\partial^2 \phi}{\partial t^2} = -\frac{E_{\perp}}{m} \frac{\epsilon}{q^2 R_0^2} \phi = -\left(\frac{v_{\perp}^2 \epsilon}{2 R_0^2 q^2}\right) \phi$$

Hence,

$$\omega_b = \sqrt{\frac{\epsilon}{2} \frac{v_{\perp}}{q R_0}} \quad (\text{A5.1})$$

This requires correction for the distortion due to the electric field, but is in any case a small amplitude approximation usually taken in the literature to apply at large amplitudes. Clearly when the poloidal excursion is large, the motion is far from an ideal SHM due to the tendency for the particle to stagnate near the zero-gradient regions, which in situations with a finite electric field is particularly marked at the downstream end of the potential well. The periodic time of the orbit,  $T_b$ , has been evaluated numerically for various zero-velocity starting points and for an array of  $x$  values given by  $x = \{0.0, 0.1, 0.2, 0.3, 0.5, 0.7, 0.8, 0.9, 0.95, 0.99\}$ , as shown in figure A5.1. All the results, actually evaluated for the half-period between reflections, are normalised using the standard result for  $T_b = 2\pi/\omega_b$ , taking  $\omega_b$  from the formula given in Eq.(A5.1), that is without considering the electric field.

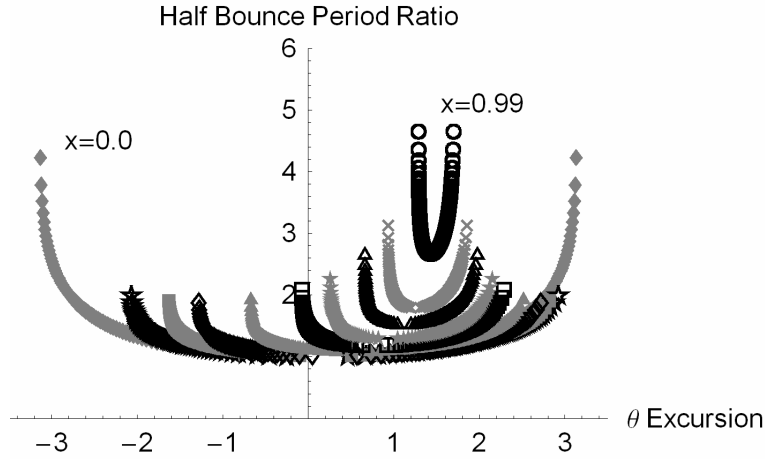


Figure A5.1: Half bounce period ratio versus poloidal angle of reflection point (ie. zero-velocity launch point) for a range of values of the normalised electric field  $x = \{0.0, 0.1, 0.2, 0.3, 0.5, 0.7, 0.8, 0.9, 0.95, 0.99\}$ . The curves corresponding to  $x=0$  and  $x=0.99$  are labelled explicitly in the graph, with the other curves corresponding respectively to the  $x$  values in between.

It can be seen that the trend is as expected in that the large amplitude excursions have significantly longer periodic times than the small ones, while increasing the value of  $x$  (the normalised electric field) causes an increase in periodic time with much the same magnitude of effect.

It is instructive to consider the effect on periodic time of tilting a sinusoidal potential energy (PE) curve. If the PE curve is an inverted cosine, then the restoring force is a sine function and the force per unit displacement (identified with  $\omega^2$  in a SHM oscillator) is a cosine. Thus displacing the minimum of the PE curve causes the average force per unit displacement to reduce, following the cosine variation, in turn reducing the oscillation frequency.

In the situation of interest, the minimum of the PE curve has moved to the point where  $\theta = \arcsin(x)$ . Here,  $\cos \theta = \cos(\arcsin(x)) = \sqrt{1-x^2}$ . Since the force per unit displacement is identified with  $\omega_b^2$ , this means that  $\omega_b \propto (1-x^2)^{1/4}$  and  $T_b \propto (1-x^2)^{-1/4}$ . Inspection of the figure A5.1 shows that this is indeed the case, valid for all values of  $x$ .

Neglecting the very small population of particles exploring the stagnation region near the crest of the PE curve, an approximate expression for the average of the bounce times can be inferred taking the ratio between the half bounce periods given by 1.2 times the minimum in each case. The average bounce period is thus approximately given by:

$$T_b(r) \approx 2.4\pi (1-x(r)^2)^{-1/4} \sqrt{\frac{2}{\epsilon}} \frac{R_0 q(r)}{v_{\perp}} \quad (\text{A5.2})$$

## Figure Captions

**Neoclassical Resistivity Revisited**, by T.N.Todd, M.C.R. Andrade, G.O. Ludwig and J. G. Ferreira

Figure 1: Potential Energy Curve for different normalised electric field values “ $x$ ”. The thicker trace corresponds to the critical value  $x_c=0.7246$  for  $\theta=0$ .

Figure 2: Trapped particle boundaries in velocity space for various values of the normalised electric field  $x$ . The dots indicate the chosen values of  $v_{\perp c}$ , and the dashed lines represent the boundary when  $E_{\phi} = 0$ .

Figure.3: Trapped particle fraction for various central electron temperatures under the effect of the toroidal electric field, and in the case when there is no electric field (crosses). In this figure only outboard midplane launch points are considered.

Figure 4: Variation of  $f_t$  with inverse aspect ratio in linear scale and fixed values of “ $h$ ”. The plot compares  $f_t$  when the complete or approximated forms for  $E_{//c}$  are used in the calculation.

Figure 5: Variation of  $f_t$  with inverse aspect ratio in logarithmic scale and fixed values of “ $h$ ”. The plot compares  $f_t$  when the complete or approximated forms for  $E_{//c}$  are used in the calculation.

Figure 6: Variation of  $f_t$  with “ $h$ ” for fixed inverse aspect ratios  $\epsilon=0.01$  (a) and  $\epsilon=0.1$  (b), comparing the complete and approximated forms for  $E_{//c}$  employed in the  $f_t$  calculation.

Figure 7: Comparison of the trapped particle fraction in the presence of the driven electric field for  $T_{e0} = 50$  eV (a), and  $T_{e0} = 2$  keV (b), obtained when the complete (eq.14) or approximated (eq.15) forms for  $E_{//c}$  are employed. In these cases launch point averaging is taken into account.

Figure 8: Current density profiles with electric field detrapping and constant temperature profile peaking factors  $\alpha_T=2$ . The graphs are obtained for different central electron temperatures.

Figure 9: Current density profiles with electric field detrapping and constant edge  $q(a) = 5.51$ . The profiles are shown for different central electron temperatures as listed in the figure.

Figure 10: Normalised central current density with both collisionality and electric field terms, with one at a time, and with neither. The thicker full trace corresponds to the case where the electric field is considered alone. The “conventional” traces are obtained for  $f_t$  calculated for a launch point at the outer midplane (NONE) and without correction to the bounce frequency due to the presence of the electric field (COLL).

Figure A3.1: Relative errors between the approximated and complete calculations for  $f_t$  against “ $h$ ” and for fixed values of the inverse aspect ratio  $\epsilon$ .

Figure A5.1: Half bounce period ratio versus poloidal angle of reflection point (ie. zero-velocity launch point) for a range of values of the normalised electric field  $x=\{0.0, 0.1, 0.2, 0.3, 0.5, 0.7, 0.8, 0.9, 0.95, 0.99\}$ . The curves corresponding to  $x=0$  and  $x=0.99$  are labelled explicitly in the graph, with the other curves corresponding respectively to the  $x$  values in between.